JACS
JOURNAL OF THE AMERICAN CHEMICAL SOCIETY

Article

pubs.acs.org/JACS

Supramolecular Assemblies of Ferrocene-Hinged Naphthalenediimides: Multiple Conformational Changes in Film States

Atsuro Takai,[*,†] Takashi Kajitani,[‡,§] Takanori Fukushima,[‡] Keiki Kishikawa,[∥] Takeshi Yasuda,[†] and Masayuki Takeuchi[*,†]

[†]International Center for Young Scientists, Semiconductor Nano-interfaces Group, and Molecular Design & Function Group, National Institute for Materials Science (NIMS), 1-2-1 Sengen, Tsukuba, Ibaraki 305-0047, Japan

[‡]Laboratory for Chemistry and Life Science, Institute of Innovative Research, Tokyo Institute of Technology, 4259 Nagatsuta, Midori-ku, Yokohama 226-8503, Japan

[§]RIKEN SPring-8 Center, 1-1-1 Kouto, Sayo, Hyogo 679-5148, Japan

[∥]Department of Applied Chemistry and Biotechnology, Graduate School of Engineering, Chiba University, 1-33 Yayoi-cho, Inage-ku, Chiba 263-8522, Japan

Supporting Information

ABSTRACT: We design a new naphthalenediimide (NDI) π-system, **NDI−Fc−NDI**, having a ferrocene linker as a hinge unit and long alkyl chains as supramolecular assembling units. The NDI units are "directionally flexible" in concert with the pivoting motion of the ferrocene unit with a small rotational barrier. The NDI units rotate around the ferrocene unit faster than the NMR time scale in solution at room temperature. UV−vis absorption, synchrotron X-ray diffraction, and atomic force microscope studies reveal that **NDI−Fc−NDI** forms a fibrous supramolecular assembly in solution (methylcyclohexane and highly concentrated chloroform) and film states, wherein the NDI units are in the slipped-stack conformation. The **NDI−Fc−NDI** supramolecular assembly in the film state exhibits multiple phase transitions associated with conformational changes at different temperatures, which are confirmed by differential scanning calorimetry, polarized optical microscopy, and temperature-dependent X-ray diffraction. Such thermal transitions of **NDI−Fc−NDI** films also induce changes in the optical and electronic properties as revealed by UV−vis absorption and photoelectron yield spectroscopies, respectively. The thermal behaviors of **NDI−Fc−NDI**, realized by the unique molecular design, are considerably different from the reference compounds such as an NDI dimer connected with a flexible 1,4-butylene linker. These results provide us with a plausible strategy to propagate the molecular dynamics of the π-system into macroscopic properties in film states; the key factors are (i) the supramolecular alignment of molecular switching units and (ii) the directional motion of the switching units perpendicular to the supramolecular axis.

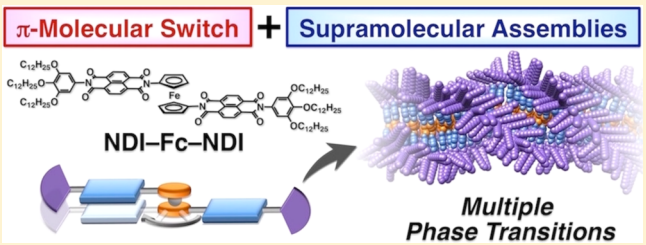

INTRODUCTION

Molecular switches are one of the simplest molecular machines in which the structure or conformation changes upon external stimuli, leading to switching of the molecular functions.[1] Switching the macroscopic properties of molecular machine assemblies in film states is regarded as an ultimate goal in chemistry and materials science.[1,2] Molecular switches comprising π-conjugated molecules, in particular, have attracted considerable attention due to their potential use as electronic and optical devices whose functions can be controlled in a designed fashion.[1,3] Most of the molecular switches to date, however, have been demonstrated in solution. This is because it is difficult to maintain the dynamic behavior of molecular switches in film states owing to the small free volume and large π-orbital overlap among the condensed molecular switches. To overcome these difficulties, molecular switches have been incorporated in crystals,[4] liquid crystals,[5] and metal−organic frameworks;[6] such switches have been reported to exhibit molecular-based dynamic behavior in condensed phases. In these systems, the movable components are well aligned or isolated, thereby facilitating the conformational change that occurs upon external stimuli such as temperature, light, and redox. Against this background, we aim to construct well-aligned supramolecular π-assemblies containing molecular switching units.

The supramolecular approach is a common, established method to align π-conjugated molecules.[7] For instance, π-conjugated macrocyclic compounds with supramolecular assembling units often form linearly assembled structures

Received: June 7, 2016
Published: August 26, 2016

DOI: 10.1021/jacs.6b05824
J. Am. Chem. Soc. 2016, 138, 11245−11253

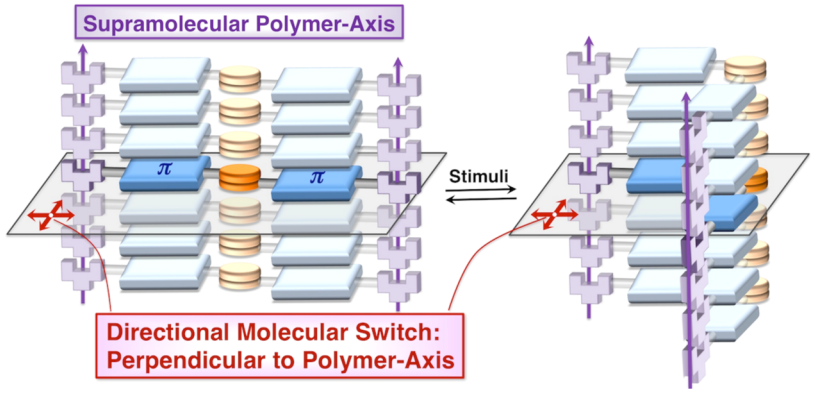

Figure 1. Schematic illustration of supramolecular assembly of π-molecular switches.

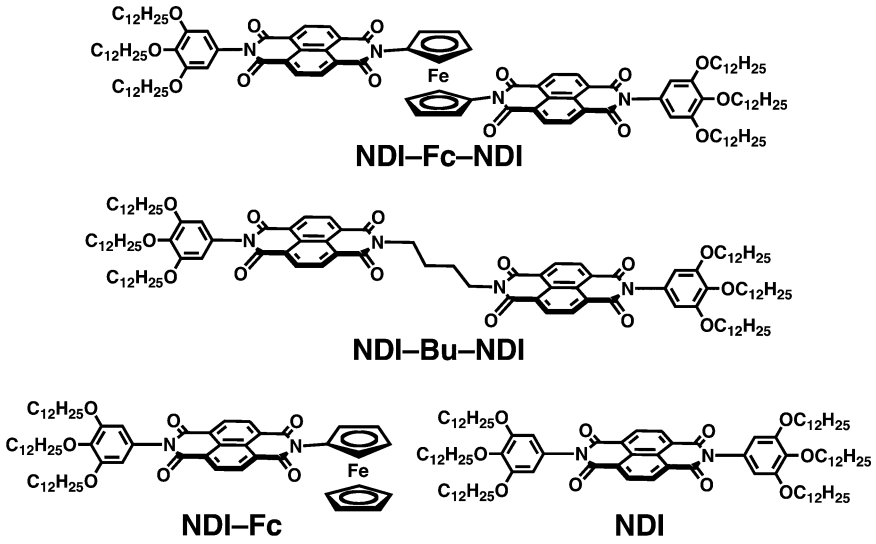

Figure 2. Structures of **NDI–Fc–NDI**, **NDI–Bu–NDI**, **NDI–Fc**, and **NDI**.

such as columnar structures. In the case of such a linear supramolecular assembly, the linear-chain axis is oriented parallel to the direction of the noncovalent interactions. We conceived the idea that π-conjugated molecules having supramolecular assembling units and directionally movable units, whose motion is independent of the supramolecular linear-chain axis, can afford a supramolecular assembly in which the flexibility of the movable units is maintained (Figure 1). Such a supramolecular assembly of π-molecular switches would induce synergetic molecular motion, resulting in macroscopic configuration changes and phase transitions in the condensed phase.[8] Previously, we successfully demonstrated that an in-solution molecular switch in which two naphthalenediimide (NDI) units are directly connected with ferrocene as a hinge unit undergoes dramatic conformational changes upon external stimuli such as redox and temperature.[9] The pivoting motion of the ferrocene unit elicits "directional flexibility" of the NDI units in this molecular switch.[9,10] Here, we expand this molecular design to prepare supramolecular assemblies of π-molecular switches by introducing assembling units into the NDI units.

The designed molecules including the reference compounds for comparison are shown in Figure 2. Two NDI units harnessed by ferrocene (**NDI–Fc–NDI**) are decorated with tridodecyloxyphenyl substituents at the imide nitrogens of the NDI units because such long alkyl chains with π-core units tend to form supramolecular assemblies through van der Waals interactions as well as π–π interactions.[11] The axis of the noncovalent interactions is perpendicular to the directional motion of the NDI units, and thus the directional flexibility of the NDI units would be maintained. Another NDI dimer connected with a flexible 1,4-butylene linker (**NDI–Bu–NDI**), a monomeric NDI with two tridodecyloxyphenyl substituents (**NDI**), and an asymmetric NDI substituted by a tridodecyloxyphenyl group and a ferrocene moiety (**NDI–Fc**) were also prepared to clarify the importance of the ferrocene rotational unit and directionally flexible NDI units of **NDI–Fc–NDI**. We have found that **NDI–Fc–NDI** supramolecular assembly formation in the solution and film states results in unprecedented multiple phase transitions which lead to **NDI–Fc–NDI** exhibiting different optical/electronic properties and conformation in each phase. Through extensive comparison with the reference compounds, the present study demonstrates the unique properties of **NDI–Fc–NDI** that allow the directional molecular motion of the π-systems in the supramolecular assemblies to translate into macroscopic configuration changes even in film states.

EXPERIMENTAL SECTION

Materials. All reagents were obtained from appropriate commercial sources (Sigma-Aldrich, Tokyo Chemical Industry, Wako Pure Chemical Industries, and Kanto Chemical) and used as received

DOI: 10.1021/jacs.6b05824
J. Am. Chem. Soc. 2016, 138, 11245–11253

Scheme 1

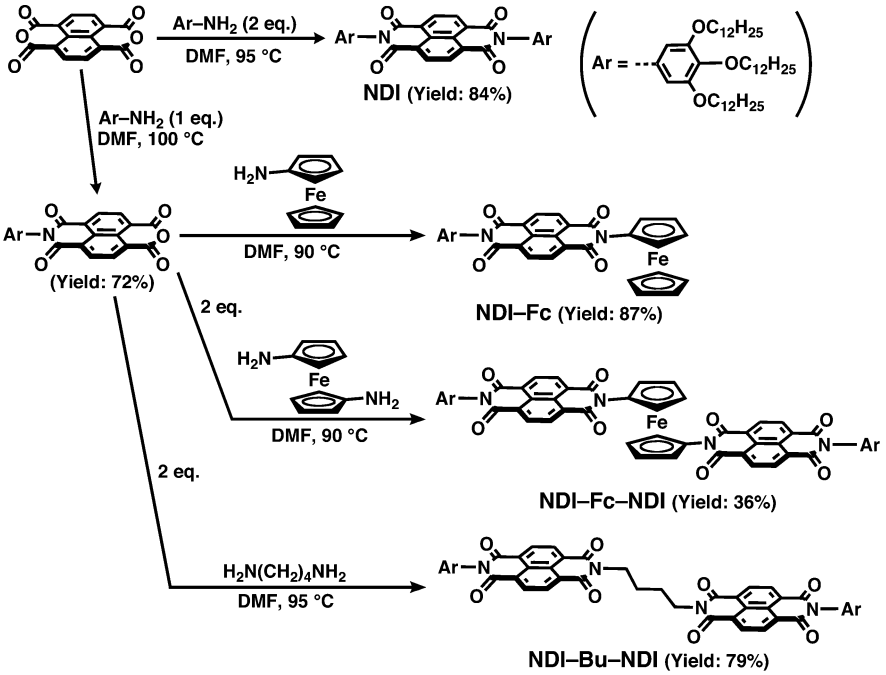

unless otherwise noted. Anhydrous solvents (chloroform, $CHCl_3$; methylcyclohexane, MCH; methanol, MeOH; dimethylformamide, DMF) were used in all experiments.[12] Diaminoferrocene,[13] 3,4,5-tridodecyloxyaniline,[14] and *N*-(3,4,5-tridodecyloxyphenyl)-1,4,5,8-naphthalenetetracarboxylic monoanhydride[15] were synthesized according to the literature, respectively. The synthetic methods and characterization data for a series of compounds presented in this study are provided in the Supporting Information.

General Procedure. Target compounds were purified by a recycling preparative HPLC (LC-9201, Japan Analytical Industry) equipped with gel permeation chromatography columns (JAIGEL-1H + 2H). NMR spectra were recorded on a JEOL ECS-400 spectrometer. Chemical shifts are expressed in ppm relative to $CHCl_3$ (7.26 ppm for ^{1}H NMR and 77.36 ppm for ^{13}C NMR).[16] UV–vis absorption spectra were recorded on a JASCO V-670 spectrophotometer in transmission mode. Differential scanning calorimetry (DSC) was carried out on a Hitachi DSC 7000x under a nitrogen atmosphere. The sample was encapsulated in a sealed aluminum pan, and an identical empty pan was used as the reference. The DSC data were obtained during the second heating/cooling cycles at a scan rate of 5 °C/min. The phase transitions and optical textures were also investigated by using a polarized optical microscope (POM), Olympus BX51, equipped with a digital camera (Olympus DP73) and a heating stage (Linkam LTS350). The POM samples were sandwiched between two glass plates. The atomic force microscope (AFM) images were recorded on a JEOL JSPM-5200 under ambient conditions at 25 °C. The samples were spin coated on silicon (100) wafers. Thermogravimetric analysis (TGA) was conducted with a Bruker AXS TG-DTA 2000SR at a heating rate of 10 °C/min under flowing argon gas. The sample was placed in an aluminum pan, and Al_2O_3 powder in an identical pan was used as the reference. The ionization potentials of solid samples obtained by drop-casting from an MCH solution were determined by a photoelectron yield spectrometer (Riken Keiki AC-3). The solid samples were annealed at each temperature for 10 min and rapidly cooled to room temperature.

Theoretical Calculations. Computational analysis and graphical representation were carried out with Spartan'14 software running under a Windows operating system. Optimized equilibrium geometries and the molecular orbitals were obtained with DFT (B3LYP/6-31G* level) methods.

Synchrotron X-ray Diffraction Experiments. Small-angle X-ray scattering (SAXS) and wide-angle X-ray diffraction (WAXD) patterns of solid samples and grazing incidence X-ray diffraction (GI-XRD) images of **NDI–Fc–NDI** film samples were obtained using the BL45XU beamline at SPring-8 (Hyogo, Japan) equipped with an R-AXIS IV++ (Rigaku) imaging plate area detector or with a Pilatus3X 2M (Dectris) detector. The scattering vector, $q = 4\pi \sin\theta/\lambda$, and the position of incident X-ray beam on the detector were calibrated using several orders of layer reflections from silver behenate (d = 58.380 Å), where 2θ and λ refer to the scattering angle and wavelength of the X-ray beam (1.0 Å), respectively. The sample-to-detector distances for WAXD and GI-XRD measurements were 0.5 and 0.4 m, respectively. The obtained scattering/diffraction images were integrated along the Debye–Scherrer ring to afford one-dimensional intensity data using the FIT2D software.[17] The lattice parameters were refined using the CellCalc ver. 2.10 software.[18]

RESULTS AND DISCUSSION

Synthesis and Conformational Dynamics of NDI–Fc–NDI in Solution. A series of NDI compounds were synthesized through a typical imide formation reaction between carboxylic anhydride and amine in DMF, as shown in Scheme 1.[19] The hetero-*N*-substituted NDI compounds (**NDI–Fc**, **NDI–Fc–NDI**, and **NDI–Bu–NDI**) were prepared in two steps: (i) monoimide formation using tridodecyloxyaniline and (ii) diimide formation using aminoferrocene (**NDI–Fc**), diaminoferrocene (**NDI–Fc–NDI**), and 1,4-diaminobutane (**NDI–Bu–NDI**).[9,20] All the compounds are fairly soluble in conventional organic solvents such as $CHCl_3$ and were characterized by ^{1}H and ^{13}C NMR spectroscopy and elemental analysis (see Supporting Information). Note that all compounds are thermally stable under experimental conditions, as evidenced by TGA thermograms (see Figure S1).

Figure 3 shows ^{1}H NMR signals of the NDI compound series in the aromatic region in $CDCl_3$ at 25 °C. A singlet peak for **NDI** and two doublet peaks for **NDI–Fc**, **NDI–Bu–NDI**, and **NDI–Fc–NDI** are assigned to the naphthalene protons. The naphthalene proton peaks of **NDI–Fc–NDI** (8.22 and 8.29 ppm) are significantly upfield shifted and much broader

DOI: 10.1021/jacs.6b05824
J. Am. Chem. Soc. 2016, 138, 11245–11253

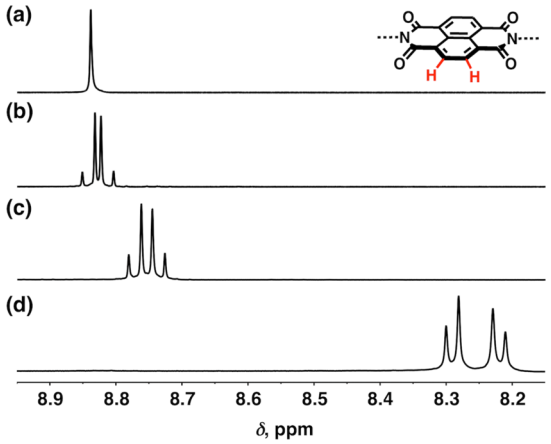

Figure 3. ^{1}H NMR spectra of (a) **NDI**, (b) **NDI–Fc**, (c) **NDI–Bu–NDI**, and (d) **NDI–Fc–NDI** in the range 8.15–8.95 ppm (naphthalene protons) in $CDCl_3$ (5×10^{-3} M) at 25 °C.

compared to the others. Such characteristic NMR signals indicate the existence of two different conformations of **NDI–Fc–NDI**: the closed form in which the two NDI units stack in a cofacial fashion with π-orbital overlap, and the open form in which the two NDI units have no π-orbital overlap (see Figure S2). The averaged signals of the open and closed forms result from the rotation of the NDI units around the Fc unit being faster than the NMR time scale (on the order of milliseconds) owing to the small rotational barrier at 25 °C. This rotational motion of the NDI units becomes slower with a decrease in temperature, as is confirmed by further broadening of the naphthalene proton peaks (see Figure S3). Note that the possibility of intermolecular NDI stacking in $CDCl_3$ can be ruled out under NMR experimental conditions based on no change in the **NDI–Fc–NDI** chemical shifts at different concentrations (5×10^{-3} M and 5×10^{-4} M). The aggregation behavior of **NDI–Fc–NDI** at much higher concentrations in a nonpolar solvent or in film states is described later.

UV–vis absorption spectroscopy also indicates the equilibrium between the different conformations of **NDI–Fc–NDI** in $CHCl_3$. The UV–vis absorption spectra of the NDI compound series (5×10^{-5} M in $CHCl_3$) are shown in Figure 4. The **NDI**, **NDI–Fc**, and **NDI–Bu–NDI** compounds have two absorption bands at 358 and 377 nm with a shoulder

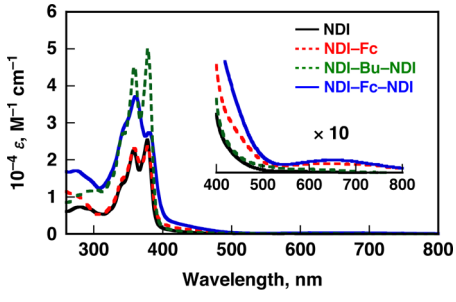

Figure 4. UV–vis absorption spectra of **NDI** (black line), **NDI–Fc** (red dashed line), **NDI–Bu–NDI** (green dashed line), and **NDI–Fc–NDI** (blue line) in $CHCl_3$ at 25 °C. In addition to the absorption bands below 400 nm, there are broad absorption bands at 644 and 648 nm for **NDI–Fc** and **NDI–Fc–NDI**, respectively. These absorption bands are assigned to the charge-transfer band between the electron donor (Fc) and acceptor (NDI), indicative of electronic interaction between the Fc and NDI moieties.

around 341 nm, which are characteristic of NDI compounds.[19] The absorption coefficient (ε) of **NDI–Bu–NDI** is almost double that of **NDI** at any wavelength in the range 250–800 nm, indicating that each NDI moiety of **NDI–Bu–NDI** behaves as a monomeric NDI. The DFT (B3LYP/6-31G* basis set) calculation supports the result that there is little interaction between the NDI units in **NDI–Bu–NDI** (see Figure S4). In contrast, the absorption of **NDI–Fc–NDI** is broadened compared to the other compounds, which may result from the mixture of the open and closed conformations. The absorption maxima of **NDI–Fc–NDI** are slightly red-shifted (361 and 380 nm), indicating that the NDI moieties stack in a slipped-cofacial fashion in the closed form.[21] This *J*-type molecular orientation is also supported by a DFT calculation (see Figure S2b). The mean-plane distance and slip angle between the NDI π-planes are 3.7 Å and 8.5°, respectively. The slipped-stack form is slightly more stable than the open form by 7.2 kJ/mol.

Aggregation Behavior of NDI–Fc–NDI in Solution and Film States. We then studied the supramolecular assembly formation of **NDI–Fc–NDI** by UV–vis absorption spectroscopy as a function of temperature. Figures 5a and 5b show the UV–vis absorption spectral changes in MCH at various temperatures. The absorption spectra change abruptly at 36 °C upon cooling with clear isosbestic points. The nonsigmoidal transition of the UV–vis absorption with the elongation temperature (T_e = 36 °C) is a characteristic of a supramolecular assembly formation via a cooperative mechanism (for details see Figure S5).[22] The T_e clearly separates the nucleation and elongation processes, and the spectral change below T_e strongly indicates elongation of the **NDI–Fc–NDI** supramolecular assembly through the NDI π-stacking and van der Waals interactions among the tridodecyloxyphenyl side chains.[23] Absorption at 299 nm appears upon formation of the supramolecular assembly and can probably be attributed to the intermolecular, rather than intramolecular, NDI π-stacking with strong electronic coupling.[21a,23] The supramolecular assembly of **NDI–Fc–NDI** was further studied through AFM observation. The sample was prepared by spin-coating an MCH solution onto a Si(100) substrate. The AFM image of the **NDI–Fc–NDI** film sample shows fibrous structures with an average height of ca. 4 nm, as shown in Figure 5c.

The supramolecular assembly formation of **NDI–Fc–NDI** was not observed in $CHCl_3$ under UV–vis or NMR spectroscopic conditions. However, a highly concentrated $CHCl_3$ solution of **NDI–Fc–NDI** exhibits optical textures under a POM, and serpentine trajectories appear when the optical textures are gently sheared (Figure 6). The trajectories are observable only under crossed Nicols, indicating that the **NDI–Fc–NDI** macrostructure is not derived from a mechanical defect but optical anisotropy. Such banded textures are typically observed for liquid crystalline supramolecular polymers;[24] thus, **NDI–Fc–NDI** forms lyotropic supramolecular assemblies in highly concentrated $CHCl_3$ as well as MCH.

Thermal Behavior of NDI–Fc–NDI in Film States. We also investigated the thermal behavior of solid samples of the **NDI–Fc–NDI** supramolecular assemblies using DSC, POM, and variable-temperature UV–vis absorption spectroscopy. The **NDI–Fc–NDI** solid samples were prepared by reprecipitation from $CHCl_3$ and MeOH, or drop-casting from MCH and $CHCl_3$ solution. It should be noted that all the data for the **NDI–Fc–NDI** solid samples shown below are, unless

DOI: 10.1021/jacs.6b05824
J. Am. Chem. Soc. 2016, 138, 11245–11253

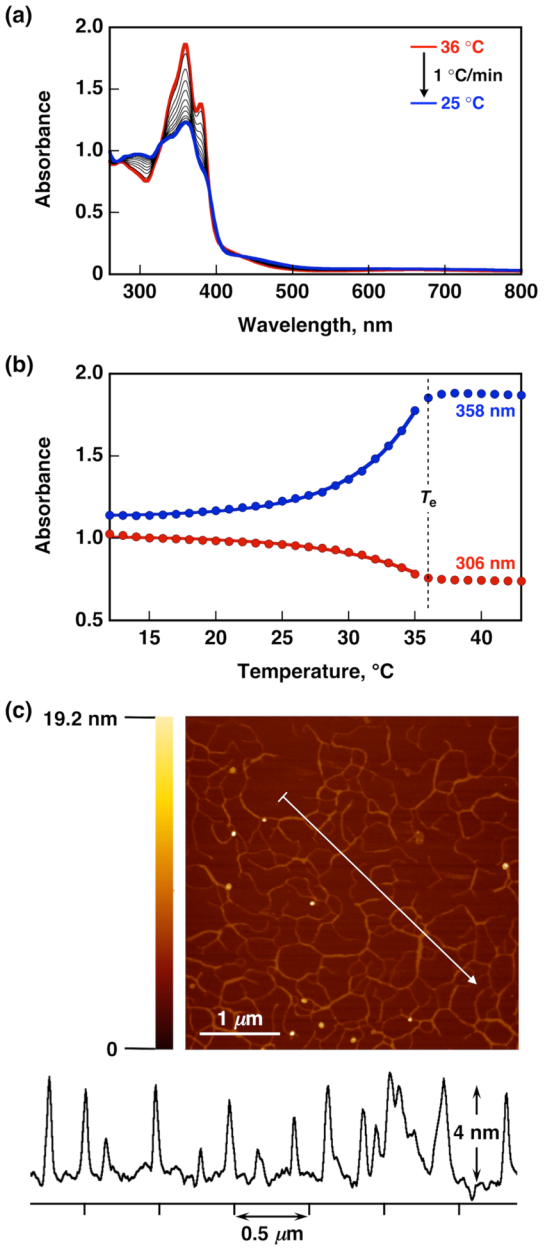

Figure 5. (a) UV−vis absorption spectral changes of an MCH solution of **NDI−Fc−NDI** (5×10^{-5} M) at various temperatures upon cooling (1 °C/min). (b) The absorbance changes at 306 nm (red) and 358 nm (blue), fitted with a cooperative model (solid lines). (c) AFM image of **NDI−Fc−NDI** supramolecular fibers at 25 °C (scale bar: 1 μm), and the cross-section profile of the fiber.

otherwise stated, basically identical irrespective of the preparation methods. The DSC, POM, and XRD measurements were also conducted for **NDI−Fc** and **NDI−Bu−NDI** to compare the thermal behaviors.

The DSC profiles and the corresponding data for **NDI−Fc−NDI**, **NDI−Fc**, and **NDI−Bu−NDI** are summarized in Figure 7 and Table 1. The DSC profile of **NDI−Fc−NDI** shows multiple endothermic and exothermic peaks as shown in Figure 7a.[25] In the heating process, three sets of endothermic and exothermic peaks are observed before melting at 216 °C. In the cooling process, a weak, broad peak at 170 °C is observed. The sawtooth-like DSC profiles in the heating process are reproducibly observed in several cycles with different samples.[26]

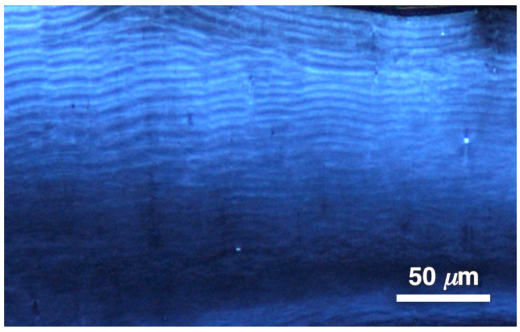

Figure 6. POM image of a concentrated $CHCl_3$ solution of **NDI−Fc−NDI** with gentle shearing on a glass substrate at 25 °C.

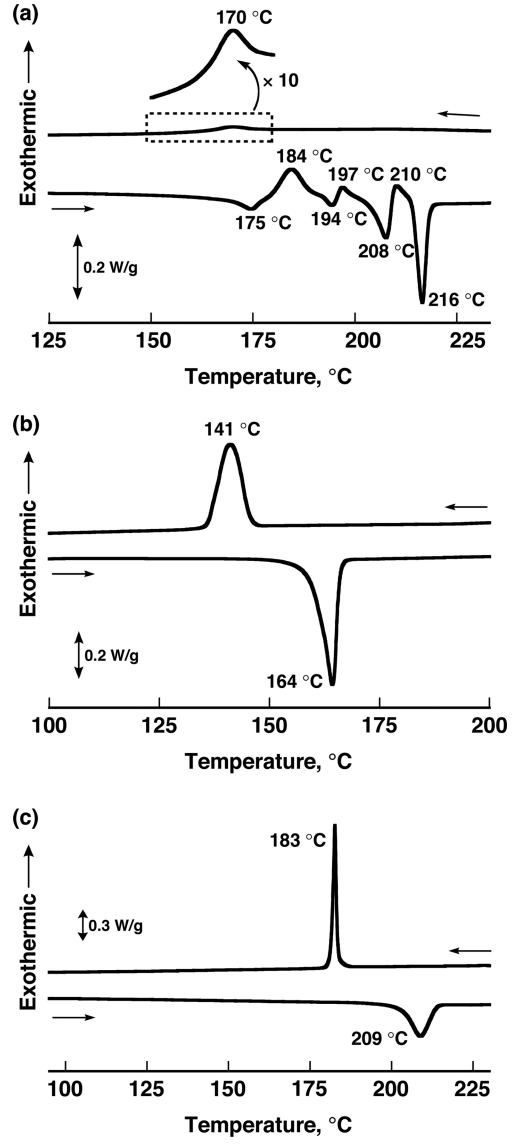

Figure 7. DSC profiles of (a) **NDI−Fc−NDI**, (b) **NDI−Fc**, and (c) **NDI−Bu−NDI** during the second heating/cooling scan at 5 °C/min.

Adjacent phase transitions are relatively close in regards to the transition temperature and transition enthalpy (ΔH). Thus, multiple phase transitions occur sequentially, alternating the configuration of the **NDI−Fc−NDI** assembly.

The POM images of **NDI−Fc−NDI** also exhibit several optical textures at different temperatures (Figure 8a), which are

DOI: 10.1021/jacs.6b05824
J. Am. Chem. Soc. 2016, 138, 11245−11253

Table 1. Phase Transition Temperatures (°C) and Enthalpies (kJ/mol, in parentheses)

compound	second heating process	second cooling process
NDI−Fc−NDI	175 (9.0) → 184 (−9.1) → 194 (1.6) → 197 (−1.5) → 208 (8.1) → 210 (−2.5) → 216 (17.2)	170 (−[a])
NDI−Fc	164 (28.3)	141 (−26.1)
NDI−Bu−NDI	209 (41.7)	183 (−38.9)

[a]Not determined precisely because of the broad peak.

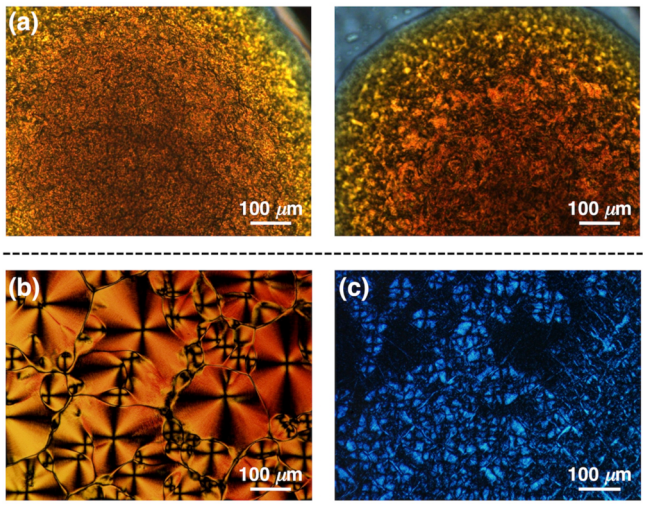

Figure 8. Polarized optical micrographs of (a) **NDI−Fc−NDI** at 184 °C (left) and 210 °C (right) upon heating from 25 °C, (b) **NDI−Fc** at 105 °C upon cooling from the isotropic melt, and (c) **NDI−Bu−NDI** at 150 °C upon cooling from the isotropic melt. The heating and cooling rate is ca. 2 °C/min. Each scale bar is 100 μm.

indicative of the multiple phase transitions among optically anisotropic states. Consistent with the DSC and POM results, the UV−vis absorption of **NDI−Fc−NDI** film samples also changes upon heating. Figure S6 shows UV−vis absorption spectra of **NDI−Fc−NDI** films annealed at different temperatures. The absorption spectrum of an **NDI−Fc−NDI** film spin-coated from a $CHCl_3$ solution at 25 °C is fairly similar to that in MCH solution at 25 °C (Figure 5a), indicating that **NDI−Fc−NDI** forms identical supramolecular assemblies in the film state and in MCH. The ratio of the absorbance at 299 nm to that at 363 nm (A_{299}/A_{363}) changes over the range 0.75 (at 25 °C) to 0.94 (at 180 °C) when the **NDI−Fc−NDI** film is annealed at different temperatures. Considering that absorption at 299 nm can probably be attributed to the intermolecular NDI π-stacking (see Figure 5), the UV−vis spectral changes of the **NDI−Fc−NDI** films may result from the different intermolecular packing structures in the **NDI−Fc−NDI** assembly. Furthermore, the electronic properties of **NDI−Fc−NDI** films also change in response to the thermal transitions, as revealed by photoelectron yield spectroscopy. The ionization potentials, that is, the negative eigenvalues of the HOMO, of **NDI−Fc−NDI** films unambiguously shift from 5.77 eV (nonannealed) through 5.67 eV (annealed at 180 °C) to 5.56 eV (annealed at 210 °C), as shown in Figure S7. The lower ionization potentials of the films annealed at higher temperatures indicate efficient electron delocalization in the **NDI−Fc−NDI** assembly.[27]

In stark contrast to **NDI−Fc−NDI**, the DSC curves of **NDI−Fc** exhibit a simple reversible phase transition with an endothermic peak at 164 °C in the heating cycle and a corresponding exothermic peak with supercooling (141 °C) in the cooling cycle (Figure 7b). POM observation of the mesophase in the cooling process (Figure 8b) reveals an optical texture with circular focal conic domains, indicating a liquid crystalline phase. No obvious phase transition from the liquid crystalline phase to a crystalline phase is observed upon cooling. Similar to **NDI−Fc**, **NDI−Bu−NDI** exhibits one mesophase upon cooling from the melt, and the POM texture with circular focal conic domains is indicative of a liquid crystalline phase (Figures 7c and 8c).

Conformational Changes of NDI−Fc−NDI Assemblies in Film States. We further conducted XRD measurements to obtain more detailed structural information on the **NDI−Fc−NDI** assemblies, **NDI−Fc**, and **NDI−Bu−NDI** in the mesophases. The conformational changes of the **NDI−Fc−NDI** assembly in film states at different temperatures were investigated by variable-temperature XRD techniques.

Figure S8 shows the XRD patterns of **NDI−Fc−NDI** solid samples prepared by drop-casting from MCH and $CHCl_3$ solutions and reprecipitation from $CHCl_3$/MeOH at 25 °C. The XRD patterns are basically the same irrespective of the sample preparation methods, indicating that identical **NDI−Fc−NDI** supramolecular assemblies are formed.

Solid samples of **NDI−Fc−NDI** obtained by drop-casting from an MCH solution exhibit XRD peaks with *d*-spacings of 7.09, 3.89, 0.67, 0.42, and 0.35 nm as well as other small peaks (Figure 9a). The GI-XRD image of an **NDI−Fc−NDI** film drop-casted from an MCH solution (Figure 9b) shows spots with a *d*-spacing of 7.09 nm in the equatorial direction (q_{xy} axis), a *d*-spacing of 3.89 nm as a broad diffraction arc in the meridional direction (q_z axis), and other *d*-spacings corresponding to the solid sample shown in Figure 9a. This result indicates that the spots with a *d*-spacing of 7.09 nm in the **NDI−Fc−NDI** assembly are perpendicular to those with a *d*-spacing of 3.89 nm. The peaks with *d*-spacings of 0.67 and 0.35 nm can be attributed to the intermolecular and intramolecular π−π stacking between the NDI units, respectively, resulting from the closed conformation of **NDI−Fc−NDI** in the assembly. The DFT calculation reveals that **NDI−Fc−NDI** has a slipped-stack arrangement between the NDI units with a 3.7 Å mean π-plane distance and 8.5° slip angle (see Figure S2b), which is reasonable in light of the XRD peaks. We infer from these results that several sets of **NDI−Fc−NDI** in the slipped-stack conformation form a discotic column, affording a helical fibrous structure. The peak with a *d*-spacing of 3.89 nm can be assigned to the diameter of the discotic column, while that of 7.09 nm, which is perpendicular to the disk plane, can be assigned to the helical pitch of the fibrous assembly. The number of molecules in a unit cell (Z) is given by the equation $Z = \rho V_{cell}/M$, where ρ (g/cm^3) is the mass density, V_{cell} ($= \pi r^2 h$) is the volume of a unit cell calculated using the columnar radius (r = 1.95 nm) and height (h = 0.67 nm), and M is the molecular weight of **NDI−Fc−NDI** (M_w = 1972.52 g/mol) divided by Avogadro's number ($N_A = 6.02 \times 10^{23}$/mol). The ρ value of organic soft materials can be assumed to be 1.0−1.2 g/cm^3;[28] thus, the Z value of **NDI−Fc−NDI** is estimated to be 2.9 for a ρ value of

DOI: 10.1021/jacs.6b05824
J. Am. Chem. Soc. 2016, 138, 11245−11253

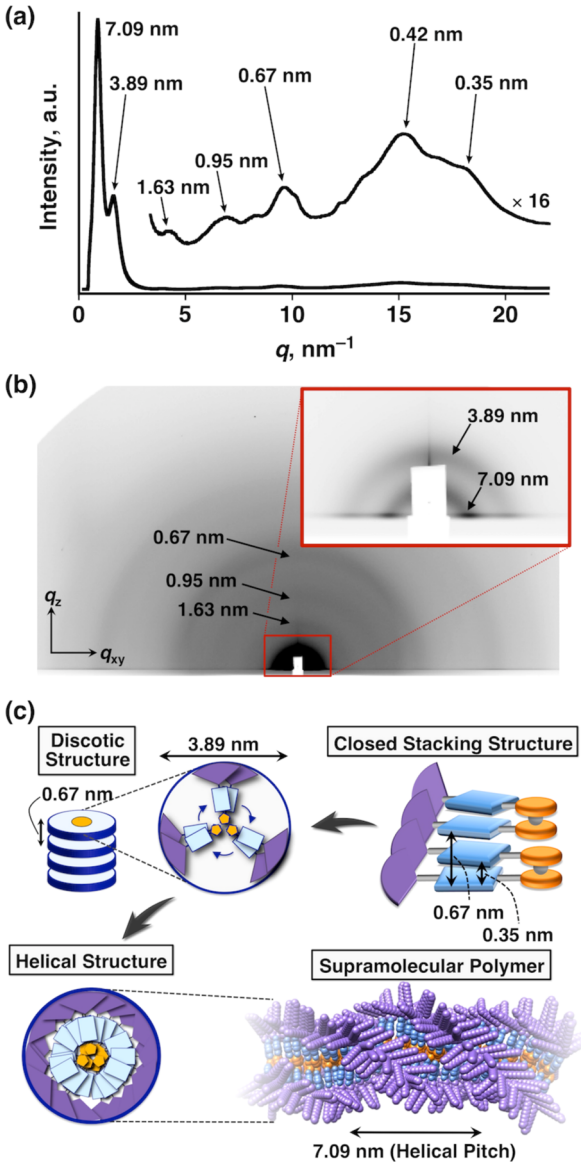

Figure 9. (a) XRD pattern of an **NDI–Fc–NDI** solid sample obtained by drop-casting from an MCH solution at 25 °C. (b) GI-XRD image of an **NDI–Fc–NDI** drop-casted film on a sapphire substrate at 25 °C. (c) Schematic illustration of the supramolecular assembled structure of **NDI–Fc–NDI**.

1.2.[29,30] These experimental data are most likely explained by the **NDI–Fc–NDI** assembled structure in which three sets of **NDI–Fc–NDI** in the slipped-stack conformation form a discotic column, finally constructing a helical fiber, as illustrated in Figure 9c. Ferrocene moieties are positioned at the center of the discotic column, and the NDI units are stacked through intramolecular and intermolecular π–π interactions as well as van der Waals interactions among the long alkyl side chains. Such a segregated stacking structure between the NDI and ferrocene units seems reasonable in light of the single-crystal structure of analogous NDI-ferrocene conjugates.[9,31] The diameter of the discotic column (3.89 nm) is consistent with the average height profile of the **NDI–Fc–NDI** fibrous structure in the AFM image (ca. 4 nm, Figure 5c).

The variable-temperature XRD results of **NDI–Fc–NDI** reprecipitated from $CHCl_3$/MeOH are shown in Figures 10 and S9.[32] During the first heating in the range 30 to 180 °C, the

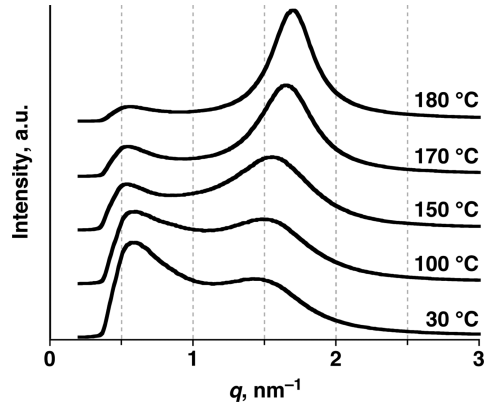

Figure 10. Variable-temperature XRD patterns (first heating) of an **NDI–Fc–NDI** solid sample obtained by reprecipitation from $CHCl_3$/MeOH.

two small-angle peaks change sequentially, while the other peaks remain almost the same. This result indicates that the supramolecular assembled structures of **NDI–Fc–NDI** are maintained but that the helical pitch and column diameter are altered. The changes in the helical pitch and column diameter are summarized in Table S3. The peak intensities of the helical pitch gradually decrease with an increase in temperature. The helical supramolecular assembly is dissociated at around 180 °C probably because of the large thermal motion of **NDI–Fc–NDI**. A number of sharp XRD peaks appear over 190 °C (see Figure S9). The XRD pattern at each temperature over 190 °C is essentially different; thus, at a minimum, three crystal-like phases exist over 190 °C.[33] These XRD observations are consistent with the DSC and POM results of **NDI–Fc–NDI**, indicating conformational changes and multiple phase transitions.

Such multistep dynamic behaviors are observed in the case of **NDI–Fc–NDI**, while **NDI–Fc** and **NDI–Bu–NDI** show only one mesophase. Together with the DSC and POM studies, the XRD studies reveal the lamellar and π-stacking structure of **NDI–Fc** (Figure 11a and Table S1) and the hexagonal columnar structure of **NDI–Bu–NDI** (Figure 11b and Table S2) in each liquid crystalline phase.

Based on the above results, we deduce that the unique molecular design of **NDI–Fc–NDI**, NDI units with two-dimensional flexibility in concert with ferrocene rotation, leads to such multistep dynamic macroscopic behaviors even in the film states. In addition, it should be noted that the sequential changes in the XRD peaks below 180 °C were not observed in the case of amorphous **NDI–Fc–NDI** films prepared by rapid cooling from the melt. This result allows us to infer that the XRD peak shifts below 180 °C are derived from the **NDI–Fc–NDI** supramolecular assemblies, and the macroscopic conformational changes of π-systems in film states are observable only for the **NDI–Fc–NDI** supramolecular assemblies. The GI-XRD results (Figure 9b) indicate that the supramolecular fibrous axis of the **NDI–Fc–NDI** assembly is perpendicular to the disk plane in which the NDI units are movable. Thus, the conformational changes of the **NDI–Fc–NDI** assembly at different temperatures can be reasonably explained by the slight directional motion of the NDI units that does not interfere with maintaining the supramolecular scaffold. As compared to the fast rotation of the NDI units of **NDI–Fc–NDI** in dilute solution (see Figure S3), the conformational changes of the **NDI–Fc–NDI** supramolecular assembly inside the films may

DOI: 10.1021/jacs.6b05824
J. Am. Chem. Soc. 2016, 138, 11245–11253

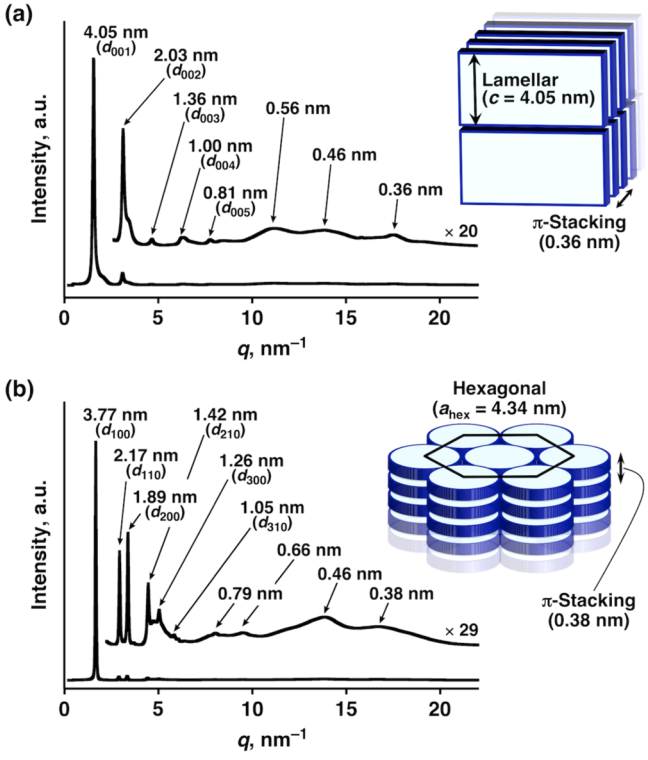

Figure 11. XRD patterns of solid samples of (a) **NDI–Fc** at 100 °C and (b) **NDI–Bu–NDI** at 150 °C upon cooling from the isotropic melts in a glass capillary (diameter: 1.5 mm). Insets represent schematic illustrations of the structural elements and parameters of the self-assembled **NDI–Fc** and **NDI–Bu–NDI**.

be small and slow owing to an increase in both the transition enthalpic and entropic factors.[6b] Nevertheless, the multiple conformational changes and related phase transitions of **NDI–Fc–NDI** strongly indicate that the transition energies between the mesophases are smaller than those of conventional rigid π-systems because of the introduction of the ferrocene hinge units and supramolecular alignment of the movable units, as illustrated in Figure S10.

CONCLUSIONS

The present study has demonstrated the dynamic behavior of a supramolecular assembly of ferrocene-hinged NDI molecules in the film state. The NDI–ferrocene conjugate works as a π-molecular switch in which the two NDI units are directionally movable in concert with the pivoting motion of the ferrocene unit with a small rotational barrier. The π-molecular switch is well aligned through supramolecular interactions including the π-stacking between the NDI units and van der Waals interactions among the long alkyl side chains. The π-molecular switch assembly exhibits multiple phase transitions, which may be related to changes in the molecular motion and intermolecular packing at different temperatures. The optical and electronic properties of the solid sample also change associated with the thermal transitions, indicating that the conformational flexibility of the π-molecular switch at the molecular level invokes macroscopic dynamic events inside the films. Thus, such supramolecular alignment of the π-molecular switch provides a promising foothold toward organic nanoelectronic and optical switches that are workable in film states. Further investigation of supramolecular assemblies and π-conjugated polymers containing hinge units is now in progress in our groups.

ASSOCIATED CONTENT

Supporting Information

The Supporting Information is available free of charge on the ACS Publications website at DOI: 10.1021/jacs.6b05824.

Details of experimental procedures, characterization, DFT calculation, various spectroscopic and the pertinent analyses data (PDF)

AUTHOR INFORMATION

Corresponding Authors

*E-mail: TAKAI.Atsuro@nims.go.jp (A.T.)

*E-mail: TAKEUCHI.Masayuki@nims.go.jp (M.T.)

Notes

The authors declare no competing financial interest.

ACKNOWLEDGMENTS

We are grateful to Dr. Takashi Nakanishi (NIMS) for his support of DSC and POM measurements, Dr. Hiroyo Segawa (NIMS) for use of TGA, Ms. Hong Gao (NIMS) for assistance with AFM, and Dr. Kenjiro Miyano (NIMS) for fruitful discussions. Synchrotron XRD experiments were carried out at the BL45XU beamline of SPring-8 with the approval of the RIKEN SPring-8 Center (Proposal Nos. 20140056 and 20150068). This research was supported by JSPS KAKENHI 15K17849 to A.T., JSPS "π-System Figuration" Project (26102009 to M.T. and 26102008 to T.F.), and MEXT "NIMS Molecule and Material Synthesis Platform" program.

REFERENCES

(1) (a) Balzani, V.; Venturi, M.; Credi, A. *Molecular Devices and Machines*; Wiley-VCH: Weinheim, 2003. (b) Saha, S.; Stoddart, J. F. In *Functional Organic Materials: Syntheses, Strategies and Applications*; Müller, T. J. J., Bunz, U. H. F., Eds.; John Wiley & Sons: Weinheim, 2007; p 295. (c) *From Non-Covalent Assemblies to Molecular Machines*; Sauvage, J.-P., Gaspard, P., Eds.; John Wiley & Sons: Weinheim, 2011. (d) *Intelligent Stimuli-Responsive Materials: From Well-Defined Nanostructures to Applications*; Li, Q., Ed.; John Wiley & Sons: New Jersey, 2013. (e) *Molecular Machines and Motors: Recent Advances and Perspectives Preface*; Credi, A., Silvi, S., Venturi, M., Eds.; Springer International Publishing: Cham, Switzerland, 2014; Vol. *354*. (f) Kottas, G. S.; Clarke, L. I.; Horinek, D.; Michl, J. *Chem. Rev.* **2005**, *105*, 1281. (g) Browne, W. R.; Feringa, B. L. *Nat. Nanotechnol.* **2006**, *1*, 25. (h) Vives, G.; de Rouville, H. P.; Carella, A.; Launay, J. P.; Rapenne, G. *Chem. Soc. Rev.* **2009**, *38*, 1551. (i) Erbas-Cakmak, S.; Leigh, D. A.; McTernan, C. T.; Nussbaumer, A. L. *Chem. Rev.* **2015**, *115*, 10081. (j) Varghese, S.; Elemans, J. A. A. W.; Rowan, A. E.; Nolte, R. J. M. *Chem. Sci.* **2015**, *6*, 6050.

(2) (a) Spruell, J. M.; Hawker, C. J. *Chem. Sci.* **2011**, *2*, 18. (b) Ariga, K.; Ji, Q.; Nakanishi, W.; Hill, J. P.; Aono, M. *Mater. Horiz.* **2015**, *2*, 406. (c) Ciferri, A. *Chem. Rev.* **2016**, *116*, 1353. (d) Lehn, J.-M. *Angew. Chem., Int. Ed.* **2015**, *54*, 3276. (e) Lutz, J.-F.; Lehn, J.-M.; Meijer, E. W.; Matyjaszewski, K. *Nat. Rev. Mater.* **2016**, *1*, 16024.

(3) (a) Muraoka, T.; Kinbara, K.; Aida, T. *Nature* **2006**, *440*, 512. (b) Ohta, E.; Sato, H.; Ando, S.; Kosaka, A.; Fukushima, T.; Hashizume, D.; Yamasaki, M.; Hasegawa, K.; Muraoka, A.; Ushiyama, H.; Yamashita, K.; Aida, T. *Nat. Chem.* **2011**, *3*, 68. (c) Hayakawa, R.; Higashiguchi, K.; Matsuda, K.; Chikyow, T.; Wakayama, Y. *ACS Appl. Mater. Interfaces* **2013**, *5*, 3625. (d) Gemayel, M. E.; Börjesson, K.; Herder, M.; Duong, D. T.; Hutchison, J. A.; Ruzié, C.; Schweicher, G.; Salleo, A.; Geerts, Y.; Hecht, S.; Orgiu, E.; Samorì, P. *Nat. Commun.* **2015**, *6*, 6330. (e) Sagara, Y.; Yamane, S.; Mitani, M.; Weder, C.; Kato, T. *Adv. Mater.* **2016**, *28*, 1073.

DOI: 10.1021/jacs.6b05824
J. Am. Chem. Soc. 2016, 138, 11245–11253

(4) (a) Khuong, T. A. V.; Nunez, J. E.; Godinez, C. E.; Garcia-Garibay, M. A. *Acc. Chem. Res.* **2006**, *39*, 413. (b) Kobatake, S.; Takami, S.; Muto, H.; Ishikawa, T.; Irie, M. *Nature* **2007**, *446*, 778. (c) Kiriya, D.; Chang, H. C.; Kitagawa, S. *J. Am. Chem. Soc.* **2008**, *130*, 5515. (d) Vogelsberg, C. S.; Garcia-Garibay, M. A. *Chem. Soc. Rev.* **2012**, *41*, 1892. (e) Shima, T.; Muraoka, T.; Hoshino, N.; Akutagawa, T.; Kobayashi, Y.; Kinbara, K. *Angew. Chem., Int. Ed.* **2014**, *53*, 7173. (f) Catalano, L.; Pérez-Estrada, S.; Terraneo, G.; Pilati, T.; Resnati, G.; Metrangolo, P.; Garcia-Garibay, M. A. *J. Am. Chem. Soc.* **2015**, *137*, 15386. (g) Naumov, P.; Chizhik, S.; Panda, M. K.; Nath, N. K.; Boldyreva, E. *Chem. Rev.* **2015**, *115*, 12440.

(5) (a) Su, X.; Voskian, S.; Hughes, R. P.; Aprahamian, I. *Angew. Chem., Int. Ed.* **2013**, *52*, 10734. (b) Yu, H.; Ikeda, T. *Adv. Mater.* **2011**, *23*, 2149.

(6) (a) Inukai, M.; Fukushima, T.; Hijikata, Y.; Ogiwara, N.; Horike, S.; Kitagawa, S. *J. Am. Chem. Soc.* **2015**, *137*, 12183. (b) Zhu, K. L.; O'Keefe, C. A.; Vukotic, V. N.; Schurko, R. W.; Loeb, S. J. *Nat. Chem.* **2015**, *7*, 514.

(7) (a) *Supramolecular Polymer Chemistry*; Harada, A., Ed.; John Wiley & Sons: Weinheim, 2012. (b) Hoeben, F. J. M.; Jonkheijm, P.; Meijer, E. W.; Schenning, A. P. H. J. *Chem. Rev.* **2005**, *105*, 1491. (c) Rybtchinski, B. *ACS Nano* **2011**, *5*, 6791. (d) Aida, T.; Meijer, E. W.; Stupp, S. I. *Science* **2012**, *335*, 813. (e) Liu, K.; Kang, Y. T.; Wang, Z. Q.; Zhang, X. *Adv. Mater.* **2013**, *25*, 5530. (f) Krieg, E.; Bastings, M. M. C.; Besenius, P.; Rybtchinski, B. *Chem. Rev.* **2016**, *116*, 2414.

(8) (a) Shibata, M.; Tanaka, S.; Ikeda, T.; Shinkai, S.; Kaneko, K.; Ogi, S.; Takeuchi, M. *Angew. Chem., Int. Ed.* **2013**, *52*, 397. (b) Yokoyama, S.; Hirose, T.; Matsuda, K. *Chem. - Eur. J.* **2015**, *21*, 13569. (c) Goujon, A.; Du, G.; Moulin, E.; Fuks, G.; Maaloum, M.; Buhler, E.; Giuseppone, N. *Angew. Chem., Int. Ed.* **2016**, *55*, 703. (d) Iwaso, K.; Takashima, Y.; Harada, A. *Nat. Chem.* **2016**, *8*, 625.

(9) Takai, A.; Yasuda, T.; Ishizuka, T.; Kojima, T.; Takeuchi, M. *Angew. Chem., Int. Ed.* **2013**, *52*, 9167.

(10) (a) Iordache, A.; Oltean, M.; Milet, A.; Thomas, F.; Baptiste, B.; Saint-Aman, E.; Bucher, C. *J. Am. Chem. Soc.* **2012**, *134*, 2653. (b) Fukino, T.; Joo, H.; Hisada, Y.; Obana, M.; Yamagishi, H.; Hikima, T.; Takata, M.; Fujita, N.; Aida, T. *Science* **2014**, *344*, 499. (c) Scottwell, S. Ø.; Crowley, J. D. *Chem. Commun.* **2016**, *52*, 2451.

(11) (a) Würthner, F.; Thalacker, C.; Diele, S.; Tschierske, C. *Chem. - Eur. J.* **2001**, *7*, 2245. (b) Reczek, J. J.; Villazor, K. R.; Lynch, V.; Swager, T. M.; Iverson, B. L. *J. Am. Chem. Soc.* **2006**, *128*, 7995. (c) Wicklein, A.; Lang, A.; Muth, M.; Thelakkat, M. *J. Am. Chem. Soc.* **2009**, *131*, 14442. (d) Percec, V.; Peterca, M.; Tadjiev, T.; Zeng, X.; Ungar, G.; Leowanawat, P.; Aqad, E.; Imam, M. R.; Rosen, B. M.; Akbey, U.; Graf, R.; Sekharan, S.; Sebastiani, D.; Spiess, H. W.; Heiney, P. A.; Hudson, S. D. *J. Am. Chem. Soc.* **2011**, *133*, 12197. (e) Dehm, V.; Büchner, M.; Seibt, J.; Engel, V.; Würthner, F. *Chem. Sci.* **2011**, *2*, 2094. (f) Hollamby, M. J.; Karny, M.; Bomans, P. H.; Sommerdijk, N. A.; Saeki, A.; Seki, S.; Minamikawa, H.; Grillo, I.; Pauw, B. R.; Brown, P.; Eastoe, J.; Mohwald, H.; Nakanishi, T. *Nat. Chem.* **2014**, *6*, 690.

(12) Armarego, W. L. F.; Chai, C. L. L. *Purification of Laboratory Chemicals*, 6th ed.; Elsevier Inc.: Oxford, 2009.

(13) Shafir, A.; Power, M. P.; Whitener, G. D.; Arnold, J. *Organometallics* **2000**, *19*, 3978.

(14) Yelamaggad, C. V.; Achalkumar, A. S.; Rao, D. S. S.; Prasad, S. K. *J. Org. Chem.* **2007**, *72*, 8308.

(15) Flamigni, L.; Baranoff, E.; Collin, J. P.; Sauvage, J. P. *Chem. - Eur. J.* **2006**, *12*, 6592.

(16) Fulmer, G. R.; Miller, A. J. M.; Sherden, N. H.; Gottlieb, H. E.; Nudelman, A.; Stoltz, B. M.; Bercaw, J. E.; Goldberg, K. I. *Organometallics* **2010**, *29*, 2176.

(17) Hammersley, A. The FIT2D Home Page. http://www.esrf.eu/computing/scientific/FIT2D/ (accessed August 6, 2016).

(18) Miura, H. CellCalc Software (version 2.10) Home Page, http://homepage2.nifty.com/~hsc/soft/cellcalc_e.html (accessed August 6, 2016).

(19) Bhosale, S. V.; Jani, C. H.; Langford, S. J. *Chem. Soc. Rev.* **2008**, *37*, 331.

(20) (a) Supur, M.; El-Khouly, M. E.; Seok, J. H.; Kay, K. Y.; Fukuzumi, S. *J. Phys. Chem. A* **2011**, *115*, 14430. (b) Cougnon, F. B.; Ponnuswamy, N.; Jenkins, N. A.; Pantoş, G. D.; Sanders, J. K. *J. Am. Chem. Soc.* **2012**, *134*, 19129. (c) Lin, X.; Hirono, M.; Seki, T.; Kurata, H.; Karatsu, T.; Kitamura, A.; Kuzuhara, D.; Yamada, H.; Ohba, T.; Saeki, A.; Seki, S.; Yagai, S. *Chem. - Eur. J.* **2013**, *19*, 6561.

(21) (a) Kasha, M.; Rawls, H. R.; El-Bayoumi, M. A. *Pure Appl. Chem.* **1965**, *11*, 371. (b) Molla, M. R.; Ghosh, S. *Chem. - Eur. J.* **2012**, *18*, 1290.

(22) (a) Jonkheijm, P.; van der Schoot, P.; Schenning, A. P. H. J.; Meijer, E. W. *Science* **2006**, *313*, 80. (b) Smulders, M. M. J.; Nieuwenhuizen, M. M. L.; de Greef, T. F. A.; van der Schoot, P.; Schenning, A. P. H. J.; Meijer, E. W. *Chem. - Eur. J.* **2010**, *16*, 362.

(23) (a) Das, A.; Ghosh, S. *Angew. Chem., Int. Ed.* **2014**, *53*, 1092. (b) Narayan, B.; Bejagam, K. K.; Balasubramanian, S.; George, S. J. *Angew. Chem., Int. Ed.* **2015**, *54*, 13053.

(24) Viney, C.; Putnam, W. S. *Polymer* **1995**, *36*, 1731.

(25) No obvious peaks are observed below 125 °C in both heating and cooling cycles.

(26) The change in scan rate (1 °C/min and 15 °C/min) causes slight peak shifts.

(27) Crispin, X.; Cornil, J.; Friedlein, R.; Okudaira, K. K.; Lemaur, V.; Crispin, A.; Kestemont, G.; Lehmann, M.; Fahlman, M.; Lazzaroni, R.; Geerts, Y.; Wendin, G.; Ueno, N.; Brédas, J.-L.; Salaneck, W. R. *J. Am. Chem. Soc.* **2004**, *126*, 11889.

(28) (a) Lvov, Y.; Ariga, K.; Ichinose, I.; Kunitake, T. *J. Am. Chem. Soc.* **1995**, *117*, 6117. (b) Yagai, S.; Usui, M.; Seki, T.; Murayama, H.; Kikkawa, Y.; Uemura, S.; Karatsu, T.; Kitamura, A.; Asano, A.; Seki, S. *J. Am. Chem. Soc.* **2012**, *134*, 7983. (c) *Polymer Handbook*, 4th ed.; Brandrup, J., Immergut, E. H., Grulke, E. A., Eds.; John Wiley & Sons: NJ, 1999; Vol. *1*. (d) *Liquid Crystals: Materials Design and Self-Assembly*; Tschierske, C., Ed.; Springer-Verlag: Berlin, 2012.

(29) The Z value can also be estimated from V_{cell}/V_{mol}, where V_{cell} is the volume of a unit cell (7.96 nm^3) and V_{mol} is the molecular volume. The V_{mol} of **NDI–Fc–NDI** in the slipped-stack form is 2.14 nm^3 according to the molecular modeling by Spartan'14 software; thus, the V_{cell}/V_{mol} value is calculated to be 3.7. Given the three sets of **NDI–Fc–NDI** in a unit cell, the V_{cell} value is slightly larger than the total molecular volume in a unit cell ($3V_{mol}$), as is similarly observed in other systems (ref 30).

(30) (a) Chen, Z. J.; Baumeister, U.; Tschierske, C.; Würthner, F. *Chem. - Eur. J.* **2007**, *13*, 450. (b) Cheng, X. H.; Liu, F.; Zeng, X. B.; Ungar, G.; Kain, J.; Diele, S.; Prehm, M.; Tschierske, C. *J. Am. Chem. Soc.* **2011**, *133*, 7872.

(31) Takai, A.; Sakamaki, D.; Seki, S.; Matsushita, Y.; Takeuchi, M. *Chem. - Eur. J.* **2016**, *22*, 7385.

(32) Note that the phase transition temperatures observed in variable-temperature XRD measurements are slightly different from those in the DSC and POM measurements owing to the different experimental setups.

(33) The sequential changes in XRD peaks indicate that several mesophases are mixed at one temperature, which precludes complete assignment of XRD peaks in these crystal-like phases.

DOI: 10.1021/jacs.6b05824
J. Am. Chem. Soc. 2016, 138, 11245–11253